Modelling Hg mobility in podzols: role of soil components and environmental implications

Gómez-Armesto, Antía[ab*]; Martínez-Cortizas, Antonio[c]; Ferro-Vázquez, Cruz[d]; Méndez-López, Melissa[ab]; Arias-Estévez, Manuel[a]; Nóvoa-Muñoz, Juan Carlos[ab]

[a] Área de Edafoloxía e Química Agrícola, Departamento de Bioloxía Vexetal e Ciencia do Solo, Facultade de Ciencias, Universidade de Vigo. 32004 Ourense, España.

[b] Environmental Technology and Assessment Laboratory. Campus da Auga- Campus of Ourense. University of Vigo. 32004, Ourense, Spain.

[c] Eco-Past (GI-1553), Faculty of Biology, Universidade de Santiago de Compostela. 15782 Santiago, Spain.

[d] ICArEHB-Interdisciplinary Center for Archaeology of Human Behaviour. Faculty of Human and Social Sciences. University of Algarve. 8005-139 Faro, Portugal.

*Corresponding author: angomez@uvigo.es

Keywords: high-resolution soil sampling, Hg pools, PCA, regression, podsolization

Abstract

A high-resolution soil sampling has been applied to two forest podzol (ACB-I and ACB-II) from SW Europe in order to investigate the soil components and processes influencing the content, accumulation and vertical distribution of Hg. Total Hg content (Hg_T) ranged 4 to 74 μg kg^{-1} in both soils, showing a strong decrease from the A to E horizon, peaks in Bhs horizons and a gradual decrease in Bw and BwC horizons. The total Hg pool (Hg_{TRes}) was 43 and 46 mg m^{-2}, where the Bhs horizons accounted for 46 and 38 % of the total Hg stored (ACB-I and ACB-II, respectively). A strong vertical heterogeneity in Hg_T and Hg_{TRes} throughout each horizon was observed thanks to the sampling scheme followed. Principal component analysis (PCA) and principal components regression (PCR), i.e.

using the extracted components as predictors, allowed to distinguish the soil components that account for Hg accumulation in each horizon. The obtained model accurately predicted accumulated Hg (R^2= 0.845) through four principal components (PCs). In A horizons, Hg_T distribution is controlled by total soil organic matter (PC4), whereas in E horizons the negative values of all PCs are consistent with the absence of components able to retain Hg and the corresponding very low Hg_T concentrations. Maximum Hg_T contents in Bhs horizons coincide with the highest peaks of secondary reactive Al compounds (PC2 and PC3) in both soils. The Hg_T distribution in the deepest horizons (Bw and BwC) seems to be influenced by other pedogenetic processes different from those in the upper part of the profile (A, E and Bhs horizons), being mainly controlled by crystalline Al compounds (PC3). Our findings confirm the importance of soils in the global Hg cycling, as they are able to subsuperficially stored large quantities of Hg preventing its mobilization to other environmental compartments.

1. Introduction

Mercury (Hg) is an element that naturally occurs in the Earth´s crust and its average concentration in worldwide soils varies between 20-250 μg kg^{-1} (Adriano, 2001). Mercury is a contaminant of international concern due to its harmful environmental effects as well as human health damage (Clarkson and Magos, 2006), especially in the methylated form. It is considered a global pollutant due to its ability to be transported by atmospheric air masses far away from its emission sources (Schroeder and Munthe, 1998; Driscoll et al., 2013) leading to a wide distribution among all the environment compartments –air, soils and waters.

Forest soils can act as an important Hg sink Hg (retaining up to 60 % of the Hg input, Grigal, 2003), being accumulated in the uppermost soil layers mainly through litterfall

(Gustin et al., 2008; Risch et al., 2012), but also due to its wet and dry deposition (Juillerat et al., 2012). Once Hg reaches the soil, it is adsorbed by soil components, such as reduced sulphur groups of organic matter (Skyllberg et al., 2006; Khwaja et al., 2006), and Al and Fe oxyhydroxides (Do Valle et al., 2005; Guedron et al., 2006).

Most studies have traditionally focused on the dynamics of atmospherically deposited Hg in surface soil horizons (e.g. Xin and Gustin, 2007). However, little is known about Hg fate in soils when this metal is accumulated at deeper soil layers, as happens in podzols and podzolic soils (Schwesig and Matzner, 2000; Peña-Rodríguez et al., 2014; Rózanski et al., 2016). In this sense, the true role of the different soil components and its vertical distribution in these soils remains unclear. This is an important gap, as podzols and podzolic soils are widely distributed worldwide, from temperate and boreal areas to tropical zones, covering about 485 million ha (Sauer et al., 2007).

The pedogeochemical functioning in podzols is strongly associated to the vertical migration, from the topsoil to the subsuperficial horizons, of dissolved organic matter (DOM) accompanied by Al and Fe compounds, mainly as organometallic complexes (De Coninck, 1980; Buurman and Jongmans, 2005; Ferro-Vázquez et al., 2014). This results in a large vertical heterogeneity of soil composition and geochemistry, which would determine the depth distribution of Hg in these type of soils, particularly in the illuvial horizons, as already noted by e.g. Nave et al. (2019). However, studies characterizing in detail the vertical pattern of Hg distribution in podzols and its relationship to the main soil physicochemical properties/components are lacking. This is because traditional soil sampling protocols, in which only one or two samples are collected per soil horizon identified in the field, are not adequate for this purpose. In order to achieve this, a more detailed sampling strategy, able to account for the high vertical variation in podzols composition and geochemistry is required.

73 This study performs a high-resolution characterization of the Hg vertical pattern in two
74 temperate forest podzols. The specific aims are the following: 1) to determine, in detail,
75 the vertical distribution of total and accumulated Hg using a high-resolution sampling
76 strategy; 2) identify which soil components and processes relate to Hg vertical
77 distribution in the studied podzols; and 3) determine how the components/processes are
78 influencing the Hg distribution. The results are also discussed from an environmental
79 perspective, focusing on the possible implications of podzols Hg dynamics on the global
80 Hg cycle.

81 ## 2. Material and methods

82 ### 2.1. Soil sampling and general characterization

83 The two podzols characterized in this work (ACB-I and ACB-II) have been studied
84 previously by Ferro-Vázquez et al. (2014, 2017). Briefly, the two soils are located in the
85 northern slope of Monte Acibro hill in Galicia (NW Spain), at 450 m above sea level. The
86 current climate conditions are characterized by a mean annual temperature of 11 ºC and
87 a total annual precipitation of about 1250 mm. Present forest vegetation includes
88 eucalyptus (*Eucalyptus globulus*) and shrubs (*Ulex europaeus*, *Daboecia cantabrica* and
89 *Calluna vulgaris*). The two soil profiles, developed in the same pedogenetic unit, are
90 separated 20 m (ACB-I and ACB-II).

91 Sampling was made using a high-resolution sampling strategy (5 cm-thickness samples)
92 until the BwC horizon, i.e. 140 cm in ACB-I and 100 cm in ACB-II, making a total
93 amount of 28 and 20 samples, respectively. Both soils have an A horizon rich in organic
94 matter, an albic E horizon and a Bhs horizon that can be divided in a Bhs1 (more organic)
95 and a Bhs2 layers, underlain by a Bw horizon, a BwC transitional horizon and a C horizon

96 which was not considered for the present study. The parent material is Quaternary
97 quarzitic colluvium.

98 Soil chemical data of both soils including organic matter content (SOM), characterization
99 of cation exchange complex, metal (Al, Fe)-humus complexes, Al and Fe inorganic
100 compounds and the total contents of several metals (Al, Fe, Si and Zr) were reported
101 elsewhere (Ferro-Vázquez et al., 2014), and are also available in Table S1
102 (Supplementary Material).

103 **2.2. Determination of total content, accumulation (Hg pool) and**
104 **enrichment of mercury**

105 Total Hg concentration (Hg_T) in 80 to 100 mg of soil, finely milled using an automatic
106 agate mortar (Retsch RM100, Retsch RM200), was measured by atomic absorption
107 spectroscopy after thermal combustion using a DMA-80 mercury analyser (Milestone).
108 The detection limit was 0.043 ng. All soil samples were analysed in duplicate and
109 repeated when the coefficient of variation exceeded 10%. For QA/QC purposes, standard
110 reference materials GBW 07402 (soil, 15 ± 3 μg kg^{-1}) and BCR 142R (soil, 67 ± 11 μg
111 kg^{-1}) were measured at the beginning of each analytical run and repeated every fifteen
112 samples. When they deviated more than 10%, the Hg analyser was re-calibrated and the
113 samples from the last satisfactory value were re-analysed.

114 The total Hg soil pool (Hg_{TRes}) was estimated for each sample having into account the
115 soil depth, soil bulk density and Hg concentration (Hg_T) as it is shown in Supplementary
116 Material.

117 **2.3. Statistical analyses**

A principal component analysis (PCA) was carried out with the aim of reducing the dimensionality of the database and summarizing the variability in a few components (PCs) that characterize the two soils under study. The soil properties included in PCA are listed in Table S2. All soil variables were standardized by multiplying them by the soil bulk density, resulting in accumulated values per soil volume. Varimax rotation was used because it maximizes the loadings of the variables on the extracted components. As the extracted principal components are orthogonal (i.e. independent), they are not subject to redundancy. Variables with loadings higher than 0.50 were considered relevant for each component.

In order to model how soil parameters are involved in Hg accumulation in the two profiles studied, principal components regression (PCR) was performed, that is to say a stepwise linear regression, using the principal component scores obtained in PCA as predictor variables and Hg as independent variable. The suitability of the obtained model was tested by representing the accumulated values of predicted vs observed Hg. The weight of each principal component (wPC) was obtained by multiplying the score of each component by the corresponding regression coefficient for each depth/sample.

All statistical analyses were carried out using SPSS version 25.0 software for Windows. Results were considered statistically significant when $p < 0.05$ and very significant when $p < 0.01$.

3. Results

A brief description of the general characteristics of both studied soils is shown in Supplementary Material, while a more detailed description of the soils can be found elsewhere (Ferro-Vázquez et al., 2014).

3.1. Total mercury: vertical distribution and pools

In general, total Hg concentrations (Hg_T) varied from 4 to 74 μg kg^{-1} in the two soils studied. Average Hg contents per soil horizon are shown in Table 1. The Hg_T content decreases with depth to its lowest values in the E horizons (range 6-7 μg kg^{-1}), and then it increases until the highest concentration in the spodic horizons Bhs2 (range 55-63 μg kg^{-1}). Moreover, a sharp decrease in Hg content was observed from the A to the E horizons in both soils.

The high-resolution sampling procedure allows to detect that Hg contents are heterogeneous within each soil horizon. Thus, in the A horizon of ACB-I Hg_T gradually decreases from the uppermost sample (0-5 cm) with a value of 49 μg kg^{-1} to 12 μg kg^{-1} in the bottom sample of this horizon (Figure 1). Total Hg values are low throughout the E horizon (4-9 μg kg^{-1}), although they are slightly higher in the samples between 25 and 40 cm. A similar pattern of Hg distribution was found in the A and E horizons of ACB-II. In this case, Hg_T diminishes from 31 to 19 μg kg^{-1} in the A horizon (Figure 1), whereas in the E horizon variation in Hg_T is almost negligible.

In the illuvial horizons, Hg_T values increase sharply from 12 to 50 μg kg^{-1} in the Bhs1 of ACB-I and from 17 to 66 μg kg^{-1} in ACB-II. Mercury content keeps increasing in the Bhs2 horizon of ACB-I, although less intensely (Figure 1), until its highest value at 85-90 cm (73 μg kg^{-1}), followed by an abrupt decrease in the deepest part of this horizon. The high-resolution sampling allowed us to identify a double peak of Hg_T in Bhs2 of ACB-II profile, one occurs at 40-45 cm (74 μg kg^{-1}) and another at 55-60 cm (69 μg kg^{-1}) (Figure 1). Underneath Bhs horizons, the Hg_T concentration decreases progressively through Bw and BwC horizons of both soils (to 16 μg kg^{-1} at 135-140 cm, in ACB-I BwC; and to 39 μg kg^{-1} at 95-100 cm, in ACB-II BwC).

Significant correlations ($p = 0.000$) were found between Hg_T and C_p ($r = 0.497$), Al_{ol} ($r = 0.621$), Al_{om} ($r = 0.803$), Al_{oh} ($r = 0.809$), Al_p ($r = 0.836$), Al_o ($r = 0.830$), Al_n ($r = 0.856$), Fe_p ($r = 0.609$), Fe_o ($r = 0.552$) and Fe_d ($r = 0.714$).

Total Hg pool (i.e., Hg_{TRes}) is similar in ACB-II (46 mg m^{-2}) and in ACB-I (43 mg m^{-2}), with the highest pools found in the Bhs horizons, accounting for 20 mg m^{-2} in ACB-I and 18 mg m^{-2} in ACB-II (Table S3), representing 46 % and 38 % of the total amount of Hg stored respectively. The eluvial horizons of both soils have the lowest Hg_{TRes} (2.6 and 1.2 mg m^{-2} for ACB-I and ACB-II, respectively). The Hg_{TRes} vertical distribution differs from that of Hg_T variation mainly in the A horizons. Thus, in the A horizon of ACB-I the total amount of Hg stored decreases from 1.3 mg m^{-2} (0-5 cm) to 0.7 mg m^{-2} (20-25 cm) (Figure 2). Hg_{TRes} in the eluvial horizon of ACB-I ranges from 0.6 mg m^{-2} (25-40 cm) to 0.3 mg m^{-2} (40-55 cm). Regarding ACB-II, Hg_{TRes} in the A horizon is close to 1 mg m^{-2} and around 0.4 mg m^{-2} in the entire E horizon (Figure 2).

In the Bhs1 sub-horizon of both soils, Hg_{TRes} increases sharply up to 2.4 and 3.0 mg m^{-2} in ACB-I and ACB-II, respectively. In the Bhs2 sub-horizons, Hg_{TRes} values were 4.1 mg m^{-2} in ACB-I and 3.6-4.0 mg m^{-2} in ACB-II. In the Bw and BwC horizons of ACB-I, Hg_{TRes} decreases continuously reaching the lowest value (1 mg m^{-2}) in the bottom-most sample (135-140 cm). In the Bw and BwC horizons of ACB-II, Hg_{TRes} does not show significant variation from 65 cm to the bottom-most sample (95-100 cm), resulting in these horizons a Hg storage twice than in ACB-I (Table 1). In both soils, Hg_{TRes} is significantly correlated ($r > 0.7$, $p < 0.05$) with different Al compounds (Al-humus complexes and crystalline Al) as well as Fe oxyhydroxides.

3.2. Assessment of main soil components involved in Hg_T distribution

188 The PCA extracted four components (eigenvalues > 1) that account for 91 % of the
189 variation of the soil data. The percentage of the variance explained by each component as
190 well as the loadings of the variables are shown in Table 2. PC1 and PC2 account for the
191 largest proportion of variance explained, with 29 and 27 %, respectively. Variables
192 included in PC1 are related to low stability Al-humus complexes (Al_K, Al_{La}, Al_{ol}), Fe-
193 secondary compounds (Fe_p, Fe_o, Fe_d), total Fe (Fe_T) and humified fraction of organic C
194 (C_p) (Table 2). PC2 comprised parameters related to medium and high stability Al-humus
195 complexes (Al_{Cu}, Al_{om}, Al_{oh}, Al_p), reactive Al (Al_o), total Al (Al_T) and potential soil
196 acidity (pH_K) (Table 2). PC3 explains 21 % of the total variance and is related to
197 secondary inorganic Al and Fe compounds (Al_n, Al_c and Fe_c), Si released after dissolution
198 of secondary inorganic Al and Fe compounds (Si_n, and Si_c) as well as total Zr (Zr_T), with
199 all the loadings showing positive values (Table 2). PC4 involves 14 % of the variance and
200 includes variables related to fresh SOM (C, N), as well as some influence of the humified
201 fraction of organic C (C_p), with positive loadings and total Si (Si_T) with negative loading
202 (Table 2).

203 In synthesis, PC1 reflects low stability Al-humus complexes and Fe-humus complexes,
204 PC2 medium-high stability Al-humus complexes (as well as Al hydroxides, total Al and
205 acidity), PC3 secondary Al compounds and PC4 soil organic matter content (SOM).

206 The four extracted PCs can be considered new, synthetic variables with which we
207 conducted a stepwise linear regression analysis (using the scores of the four PCs) to model
208 accumulated Hg (Hg_{acc}) distribution in the two soils. The best model included the four
209 principal components retained in PCA (Table S4), with an adjusted R^2 of 0.845. The
210 corresponding unstandardized coefficients obtained are summarized in Equation 1.

211 $$Hg_T = 38.04 + 14.40 * PC3 + 12.74 * PC2 + 7.49 * PC1 + 4.75 * PC4 \qquad Eq.\ (1)$$

212 Having into account the values of the standardized coefficients of the model, PC3 and
213 PC2 have a similar weight in the estimation of modelled Hg values (0.630 and 0.558,
214 respectively), being higher than PC1 (0.328) and almost three times higher than PC4
215 (0.208).

216 Figure 2 shows the observed and modelled patterns of accumulated Hg (Hg_{acc}) —i.e. Hg
217 values standardized by soil bulk density (see Materials and Methods section). In general,
218 the Hg_{acc} is slightly underestimated in the uppermost sample of the A horizon of both
219 soils, improving the fitting in the lower part of A horizons. In E horizons, the Hg_{acc} is
220 higher than the modelled, particularly in ACB-II. Regarding illuvial horizons, the
221 modelled amount of Hg_{acc} is higher than the measured values in the samples from Bhs1,
222 whereas the opposite occurs in most of the Bhs2 horizon for both soils. Overall, the model
223 is rather accurate with root mean-square error values (RMSE) of 4.3, 11.4, 8.9 and 4.4 for
224 A, Bhs, Bw-BwC and E horizons, respectively.

225 The weight of each PC (wPC), which reflects the influence of each component in the
226 predicted Hg_{acc} at each depth, is shown in Figure 3. A different component fractionation
227 was observed for ACB-I and ACB-II soils, particularly in the Bw and BwC horizons. In
228 the A horizon of both soils, the main soil components influencing Hg_{acc} are SOM content
229 (PC4) with positive weight, and Al, Fe and Si compounds (PC1, PC2 and PC3) with
230 negative weights. The Hg_{acc} in E horizons is related to PC1, PC2, PC3 and PC4, with
231 negative weights. In the upper part of Bhs horizon, predicted Hg_{acc} is positively influenced
232 by low stability metal (Al, Fe)-humus complexes and Fe oxyhydroxides (PC1) as well as
233 SOM (PC4). However, the fractionation in the Bhs2 horizons is quite different between
234 ACB-I and ACB-II. In ACB-I, Hg_{acc} is perceptibly influenced by medium-high stability
235 Al-humus complexes and non-crystalline Al (PC2). In contrast, in ACB-II there is a
236 gradual transition in the predominance of the components that influence Hg_{acc}, being more

237 relevant the Al and Fe-humus complexes and Al-hydroxides (PC1 and PC2) in the upper
238 part of the sub-horizon (40-50 cm) and PC2 and PC3 between 50 and 60 cm (Figure 3).
239 This contrasting behaviour of Hg_{acc} is also observed in Bw and BwC horizons of the two
240 soils. While in ACB-I it is mainly related to medium and high stability Al-humus
241 complexes (PC2), crystalline Al and Si (PC3) clearly dominate in ACB-II (Figure 3).

242 # 4. Discussion

243 ## 4.1. Total mercury: vertical distribution and pools

244 The Hg_T concentrations of the two soils studied are in the order the natural background
245 concentration in non-polluted soils (< 100 µg kg^{-1}; Xin and Gustin, 2007) and the maxima
246 also 2-4 fold lower than the maxima recorded in nearby ombrotrophic bogs (Martínez-
247 Cortizas et al., 2012).

248 The depth record of Hg_T is characterized by a bimodal distribution, with relatively high
249 contents in A and spodic horizons and low in E and BwC horizons. The concentrations
250 of Hg_T in the A horizons of ACB soils (12-49 µg kg^{-1}) are consistent with those reported
251 for A horizons of podzolic soils from previous studies which range from 10 to 60 µg kg^{-1}
252 (Do Valle et al., 2005; Richardson et al., 2013; Nave et al., 2019). In ACB soils, the role
253 of organic matter in the accumulation of Hg in the A horizons is supported by the
254 significant correlations ($n = 8$; $p < 0.01$) between Hg_T and total C ($r = 0.905$) and total N
255 ($r = 0.882$). The organic matter is widely known to have a high affinity for Hg, especially
256 for the reduced sulphur groups (Khwaja et al., 2006; Skyllberg et al., 2006; Smith-
257 Downey et al., 2010). In particular, for podzolic soils, Nave et al. (2019) reported a
258 significant correlation between Hg and total organic C in 91 podzols from U.S.

259 The very low Hg_T contents of the E horizons of the studied soils (range 4-9 µg kg^{-1}) are
260 interpreted as a consequence of the Hg depletion due to podsolization, as it was previously

261 reported in other studies (Peña-Rodríguez et al., 2014; Rózanski et al., 2016; Gómez-
262 Armesto et al., 2018).

263 The relatively high Hg_T content in the Bhs horizons of the two soils (12-74 μg kg^{-1}) is
264 consistent with the data reported for spodic horizons in the literature (Schwesig and
265 Matzner, 2000; Richardson et al., 2013; Blackwell et al., 2014; Peña-Rodríguez et al.,
266 2014; Yu et al., 2014; Rózanski et al., 2016). In all these studies, analogously to ACB
267 soils, Hg_T in the illuvial horizons shows the highest concentration of the mineral soil,
268 excluding the O or A horizons, in which total Hg is expected to be higher in soils with
269 background Hg concentrations, as reported recently by Nave et al. (2019). As for Hg,
270 subsurface peaks of other elements such as lead have been reported in different studies
271 focusing on the fate of heavy metals in podzols (Bindler et al., 2008; Ferro-Vázquez et
272 al., 2017).

273 In the deeper soil (Bw and BwC horizons), Hg_T decreases again although their values are
274 considerably higher than in E horizons in which Hg is depleted due to podsolization
275 (Figure 1). This suggests a weaker influence of the podsolization process in Hg
276 mobilization in Bw and BwC horizons compared to other parts of the soils.

277 Contrary to what is expected, the highest amount of stored Hg in ACB soils was found in
278 the spodic horizons (up to 46 % of the total Hg pool in the soil). This is attributed to the
279 illuviation process, acting spodic horizons of ACB soils as a Hg sink. The role of mineral
280 soil horizons in storing Hg was evidenced in forest soils from northeastern U.S. (Yu et
281 al., 2014) and recently reinforced by Richardson et al. (2018), who outlined a greater
282 ability of the mineral soil below 30 cm to sequester Hg compared to the uppermost soil
283 layers. In the present study, the total Hg pool in the Bhs horizons of ACB-I and ACB-II
284 (20 and 18 mg m^{-2}, respectively; Table S3) is higher than the results found by Blackwell

et al. (2014) in illuvial horizons of forest soils from New York State (9-11 mg m^{-2}). However, our results are lower than the values obtained by Larssen et al. (2008) in Bhs horizons (23 mg m^{-2}). This ability of subsuperficial horizons to accumulate Hg could imply a greater capacity of soils to contribute to terrestrial ecosystems Hg pool that has not been considered until now.

4.2. Soil components and processes influencing Hg vertical pattern

The factor contributing the most to the Hg_{acc} values in A horizons, (Figure 2) is the soil organic matter content (PC4), represented by the total organic C and N contents as well as humified organic C (C_p) (Figure 3). Its effect is somewhat higher for ACB-I than for ACB-II, probably due to a larger SOM content in the former (Table S1). In addition to a quantity factor represented by total organic C, the quality factor of SOM (C_p) is also relevant in the Hg accumulation. In this sense, the ability of SOM for Hg binding depends on its own characteristics in terms of density fractions (Nave et al., 2019), accessibility to binding sites, sorption capacity and sorption affinity, as well as the nature of DOM (Schlüter, 1997). Moreover, the strong affinity between Hg and organic matter, particularly through the reduced sulphur groups (Skyllberg et al., 2006), contributes to the accumulation of Hg in the superficial soil layers. It was also reported that at pH values between 4.0-4.7, the same range of pH values of the A horizons of ACB-I and ACB-II (Table S1), SOM is expected to be more efficient than Fe oxides and clay minerals in binding Hg (Do Valle et al., 2005; Manceau and Nagy, 2008). The weight of the organic matter factor in Hg accumulation decreases with depth within the A horizons of both soils —a fact that can be only detected with a strategy of high-resolution sampling—, which is consistent with a contribution from atmospheric deposition and/or from litter. The negative weight of secondary Fe compounds and low stability Al-humus complexes

309 (PC1), as well as secondary reactive Al compounds (PC2), suggests that Al and Fe could
310 be effective competitors against Hg for binding sites of SOM in A horizons, influencing
311 its whole ability to accumulate Hg.

312 The low amount of Hg_{acc} in E horizons is well described by the PCR model in both soils
313 (Figure 2). The Hg decline in E horizons is consistent with the depletion of metal (Al,
314 Fe)-humus complexes, secondary compounds of Fe and Al and organic matter, which are
315 actively involved in Hg retention (Schwesig and Matzner, 2000; Do Valle et al., 2005;
316 Peña-Rodríguez et al., 2014), and whose mobilization during podsolization is part of the
317 podzol formation process in temperate areas (Buurman and Jongmans, 2005; Sauer et al.,
318 2007). This is in agreement with the negative weights that show PC1, PC2 and PC4 in the
319 E horizons of both soils (Figure 3). Crystalline Al, Fe and Si compounds (Al_c, Fe_c, Si_c,)
320 which together to Zr load in PC3 (Table 2), also show a negative effect in the Hg
321 accumulation in E horizons. Secondary crystalline compounds have a lower adsorption
322 capacity compared to non-crystalline ones (Schwertmann and Cornell, 2000), but the
323 participation of both compounds showed a scarce influence in Hg retention in E horizons
324 due to their low contents (Table S3).

325 The overestimation of Hg in Bhs1 horizons of both soils could be related to secondary Fe
326 compounds (Fe_p, Fe_o, Fe_d; PC1), which is the factor that showed the greatest positive
327 weight (Figure 3). The relevance of Fe compounds in these horizons is in agreement with
328 their maxima found in the Bhs1 sub-horizons of ACB-I and ACB-II (Ferro-Vázquez et
329 al., 2014). It is also consistent with the results of other studies of Hg content and
330 accumulation in soils. For example, Navrátil et al. (2014) reported a positive correlation
331 between total Hg and oxalate-extractable Fe (Fe_o) in mineral horizons of some podzols,
332 whereas Nave et al. (2019) also indicated the participation of Fe oxyhydroxides in Hg

binding in podzols. Guedron et al. (2009) found a positive correlation between Hg and non-crystalline Fe compounds in Fe-rich B horizons, and the relationship between Hg and Fe compounds has been also reported in several studies (Do Valle et al., 2005; Grimaldi et al., 2008). Crystalline and non-crystalline Al compounds in the Bhs1 sub-horizons showed a negative weight in relation with the Hg accumulation, suggesting that these compounds are not competitive enough compared to Fe compounds in Hg retention in these horizons.

Although with a lower influence, SOM (PC4) is also involved in Hg accumulation in the Bhs1 through the humified organic C fraction (C_p). This type of organic matter provides sites for binding Hg, which is expected to be mobilized (similarly to Fe and Al) together with dissolved organic C (DOC) from uppermost soil layers. The accumulation of mobilized organic matter in the uppermost centimetres of illuvial horizons is characteristic of temperate forest podzols (Buurman and Jongmans, 2005). In this sense, Hg solubility was found to be strongly influenced by the formation of soluble Hg-DOM complexes (Schlüter, 1997). Other studies also suggested that Hg mobilization from organic horizons to deeper soil layers was controlled by its interaction with the DOC in forest podzols (Amirbahman et al., 2004), while Alriksson (2001) already mentioned the role of DOC as carrier of Hg in podsolization. The mobilization of Hg from superficial A horizons to deeper layers of podzols is also supported by modelling of batch experimental data (Schlüter and Gäth, 1997).

The Hg_{acc} levels in Bhs2 horizons of both soils are underestimated by the PCR (Figure 2), being the factors involved in the accumulation of Hg different between ACB-I and ACB-II (Figure 3). The amount of Hg in Bhs2 horizon of ACB-I seems to be related to secondary reactive Al compounds (PC2), including medium and high stability Al-humus

357 complexes (Al_{om}, Al_{oh}), in a much greater degree than the amount of SOM (PC4). The
358 weight of PC2 shows an increase with depth within the Bhs2 sub-horizon (from 70 to 90
359 cm), being consistent with the highest Hg_T value in ACB-I (85-90 cm, Figure 1). This Hg
360 peak coincides with the greatest accumulation of secondary reactive Al compounds in
361 ACB-I (Ferro-Vázquez et al., 2014). Several studies have found relatively high values of
362 Hg in subsurface horizons which were attributed to metals mobilized by DOC (Schwesig
363 and Matzner, 2000; Hissler and Probst, 2006; Larssen et al., 2008). This is in agreement
364 with batch experiments results showing the highest Hg retention capacity in Bs horizons
365 of podzols (Schlüter, 1997). However, the predicted values of Hg_{acc} in the deeper part of
366 Bhs2 of ACB-I differ from the observed values, suggesting the participation of additional
367 factors or soil components not included in the PCR.

368 In the uppermost layers of the Bhs2 of ACB-II (40-50 cm), the main factor involved in
369 Hg accumulation is the content of secondary Fe compounds (PC1), similarly to what
370 occurs in Bhs1 layer (Figure 3). This contrasts with the role of secondary reactive Al
371 compounds (PC2) in Hg retention observed in the same horizon of ACB-I. The distinctive
372 behaviour in these samples of the Bhs2 of ACB-II could be related to their greater amount
373 of Fe-humus complexes (Fe_p) and crystalline Fe oxyhydroxides (Fe_d) (Table S1). Instead,
374 in the lower section of the Bhs2 of ACB-II (50-60 cm), secondary Al compounds (Al-
375 humus complexes and crystalline and non-crystalline Al minerals) are the most important
376 factor for the vertical distribution of Hg. Iron and Al oxides were reported to be efficient
377 in terms of adsorption of Hg complexed to DOM in illuvial horizons of podzols (Schlüter,
378 1997), and Gabriel and Williamson (2004) also considered the role of Al and Fe
379 oxyhydroxides as suppliers of binding sites of organically complexed Hg. Similarly, Fe
380 and Al compounds, including metal (Al, Fe)-humus complexes, have shown a significant
381 role in Hg retention in soils (Guedron et al., 2009).

382 Unexpectedly, we did not observe a direct influence of SOM (PC4) in the vertical pattern
383 of Hg in Bhs horizons of both soils. This contrasts with the findings of Hissler and Probst
384 (2006) who considered that organic C enrichment in the soil justifies the variation of the
385 Hg content in podzolic soils, but it is consistent with the results of Nave et al. (2019) who
386 maintain that C and Hg are independently cycled in illuvial horizons. However, the
387 indirect effect of organic matter is expressed though the role of metal (Al, Fe)-humus
388 complexes which constitute PC1 and PC2. This would highlight the different role of SOM
389 in the vertical distribution of Hg in podzols, behaving mainly as a carrier in A and E
390 horizons whereas promoting Hg retention in Bhs horizons through its adsorption to
391 different Al and Fe compounds. Indeed, the mobilization of Hg as organic Hg complexes
392 towards mineral horizons, and its interaction with Al and Fe oxyhydroxides, was reported
393 by Guedron et al. (2009) in tropical soils.

394 The Bw and BwC horizons of both soils do not show a clear trend between the predicted
395 and observed Hg_{acc} (Figure 2). In the Bw and BwC horizons of ACB-I, the main factor
396 responsible for the vertical pattern of Hg in these soil layers seems to be relatively stable
397 organic Al compounds (PC2; Figure 3). The weight of PC2 in the explanation of Hg
398 pattern diminishes with soil depth, consistent with the decrease in the amount of Al-OM
399 compounds. The low contents of organic C and inorganic Al compounds in the Bw and
400 BwC horizons (compared to ACB-II) accounts for the negative weight of PC4, PC3 and
401 PC1 in the Hg distribution (Figure 3).

402 In ACB-II, the vertical distribution of Hg in Bw and BwC horizons is mainly explained
403 by the secondary crystalline Al, Fe and Si compounds (PC3). The amount of crystalline
404 Al and Fe compounds (Al_c and Fe_c) is comparatively greater than in ACB-I (Table S1).
405 Crystalline compounds of Fe and Al were reported to be efficient Hg sorbents in poorly

406 organic horizons through the formation of hydroxyl Hg species, and these compounds are
407 mostly involved in Hg retention in C horizons of podzols (Schlüter, 1997). Crystalline Al
408 hydroxides were also considered in Hg retention in ferralsols, acrisols and gleysols, due
409 to their positive correlation with Hg content (Guedron et al., 2009). The weight of
410 secondary crystalline Al, Fe and Si compounds (PC3) in the explanation of Hg content
411 increases with soil depth in ACB-II, reflecting the intensity of the weathering process.

412 Soil components involved in Hg distribution in the Bw and BwC horizons of both soils
413 are different from those in the A, E and Bhs horizons, underlining that the former are not
414 affected by podsolization (eluviation and illuviation) to a large extent. This is in
415 agreement with the results reported by Nave et al. (2019), which highlighted the role of
416 soil forming processes in Hg distribution in podzols against the common view mainly
417 focused on C-Hg interactions. This is supported by the role of metal (Al, Fe)-humus
418 complexes (Al_p, Fe_p), corresponding to PC1 and PC2, compared to the role of SOM (PC4)
419 in the vertical variations of Hg.

420 **4.3. Environmental implications of podzols into the global Hg cycling**

421 The results obtained in our study are important due to the potential environmental
422 implications in the terrestrial biogeochemical Hg cycle. The following interpretations in
423 environmental terms are also extendable to soils around the world showing similar
424 pedogenetic processes (downward mobilization of organic matter and several metals) and
425 soil components such as Al and Fe hydroxides and metal-humus complexes.

426 The removal of Hg from the uppermost soil layers as a result of podsolization constitutes
427 a natural detoxifying process occurring in the O and A soil horizons, leading to a lower
428 accumulation of Hg in surface horizons of soils from areas located far from pollution
429 sources. Thus, the downward Hg mobilization prevents its accumulation reaching critical

430 load values (130 μg kg^{-1} according to Tipping et al., 2010 and up to 320 μg kg^{-1} following
431 Frossard et al., 2017), therefore avoiding toxicity risks for small invertebrates, plants and
432 microorganisms which play a key role in the biogeochemical reactions that take place in
433 surface soil horizons. A low concentration and accumulation of Hg in surface soil layers
434 would also contribute to reduce the mobilization of soil Hg by runoff, one of the main
435 paths for Hg export in terrestrial ecosystems (Mitchell et al., 2008). Similarly, less Hg is
436 expected to be accessible for re-volatilization to the atmosphere, reducing secondary
437 natural Hg emissions (Smith-Downey et al., 2010), either as direct Hg evasion due to light
438 exposure (Xin and Gustin, 2007), non-photochemical abiotic reduction (Jiskra et al.,
439 2015), consequence of forest fires (Biswas et al., 2008) or due to changes in the land use
440 (Obrist et al., 2016).

441 Moreover, the mechanisms involved in podzolization transform spodic horizons into a
442 geochemical barrier that prevents further Hg mobilization towards groundwaters. As a
443 consequence, a lower amount of Hg is expected to reach aquatic ecosystems where it can
444 be easily methylated (Regnell and Watras, 2019).

445 On the other hand, our results show that the Hg sequestration in the illuvial horizons is
446 mainly related to metal-humus complexes, in which the rate of C mineralization is much
447 slower than non-metal-complexed soil organic matter (Schwesig et al., 2003), probably
448 due to the inhibiting effect of metals that complex the well-humified organic carbon.
449 Thus, Hg sequestered in podzol illuvial horizons will be presumably less sensitive to
450 changes in the biogeochemical cycle of C in the global warming scenario that has been
451 proposed (e.g. Smith-Downey et al. 2010), contributing to keep the soil capacity as the
452 main Hg sink in terrestrial ecosystems in podzol areas around the globe. This could
453 counterbalance the indeterminate response of surface horizons in Hg storage as a

consequence of different processes (such as land use changes, lower Hg emissions due to the Minamata Convention, fires, global warming, etc.) that can modify the lifetime of Hg in soils (Smith-Downey et al., 2010).

It is particularly remarkable the influence of deeper, mostly mineral, soil horizons (Bw and BwC) in the vertical distribution of Hg. In spite of the fact that these horizons are not directly influenced by podsolization, they retain a relevant amount of Hg complementing the sink role of illuvial horizons. Thus, the Bw and BwC layers should be taken into consideration as part of an effective strategy involving soils in order to avoid Hg pollution of groundwaters.

The Bw and BwC horizons together with the spodic horizons store relatively large amounts of Hg, that accounts for 80 and 92 % of the total Hg pool in ACB-I and ACB-II soils, respectively. These figures indicate that the global soil Hg pool could be underestimated, since most studies are focused on Hg accumulation in the superficial soil layers (i.e. 30 cm) and its interactions with SOM (Obrist et al., 2011; Richardson et al., 2013; Navrátil et al., 2014). A simple calculation of the total Hg stored in spodic horizons of podzols worldwide, assuming an average Hg pool value of 18 mg m^{-2} (the average found in this work for Bhs horizons) and taking into account that podzols cover 430 million ha of land around the globe, results in a figure in the order of 77,400 Mg of Hg stored in illuvial podzolic horizons. This amount makes approximately 7% of all total Hg globally accumulated in soils (Sunderland and Mason, 2007). This value, which is not negligible, highlights the capacity of deep soil layers to act as a global sink of Hg coinciding with Richardson et al. (2018), who showed the importance of deep soil/regolith in Hg accumulation. This fact should be considered in future studies assessing the role of soils in the biogeochemical cycle of terrestrial Hg.

5. Conclusions

The high-resolution soil sampling performed in the two podzols studied, ACB-I and ACB-II, provided detailed information on the vertical Hg distribution and the soil components and processes involved. The Hg content varies with depth, following a bimodal distribution, with the highest values in the A and Bhs horizons. This behaviour could not have been detected with a traditional sampling scheme. The Hg accumulation in Bhs horizons seems to be related to well-humified soil organic C (C_p) and metal-humus complexes, mainly Al-humus complexes, whereas Fe-humus complexes have a minor influence. The role of these soil components in the Hg distribution of both soils was confirmed by the PCR results.

The Bw and BwC horizons also accumulate a significant amount of Hg (Hg_{TRes}) in both soils, which is probably related to the role of crystalline Al compounds. This suggests that different soil processes are involved in the Hg vertical distribution, being dominated by podsolization in the A, E and Bhs horizons, while weathering of soil parent material is the dominant process for the Hg accumulation in the Bw and BwC horizons.

Mercury accumulation in illuvial horizons of podzols leads, in environmental terms, to a reduction in total Hg load in uppermost soil layers (O and A horizons), minimizing its potential toxic effects in soil biota and reducing the risks posed by changes in organic matter mineralization rates due to global warming. In addition, the soil compounds involved in Hg accumulation in Bhs horizons prevent its mobilization to groundwaters, conferring to these horizons a role as geochemical barrier against Hg downwards transport.

The findings from this study reinforce the role of soils in the biogeochemical Hg cycle and are extendable to worldwide soils whose geochemistry is dominated by interactions between SOM, metal-humus complexes and Fe and Al oxyhydroxides.

Acknowledgements

A. Gómez-Armesto acknowledges the predoctoral grant of Xunta de Galicia (ED481A-2016/220) as well as the CITACA contract (08.CITACA-2019) and M. Méndez-López acknowledges the predoctoral grant FPU of Ministerio de Educación y Formación Profesional (FPU17/05484). It is also recognized the financial support of the Consellería de Cultura, Educación e Ordenación Universitaria (Xunta de Galicia) through the contract ED431C 2017/62-GRC granted to the research group BV1 of the University of Vigo, the research project ED431F2018/06-EXCELENCIA and CITACA Strategic Partnership (ED431E 2018/07).

References

Adriano D.C. Trace elements in terrestrial environments: Biogeochemistry, bioavailability, and risks of metals. Springer, New York, 2001.

Alriksson A., 2001. Regional variability of Cd, Hg, Pb and C concentrations in different horizons of Swedish forest soils. Water Air Soil Pollut. Focus 1: 325-341.

Amirbahman A., Ruck P.L., Fernandez I.J., Haines T.A., Kahl J.S., 2004. The effect of fire on mercury cycling in the soils of forested watersheds: Acadia National Park, Maine, U.S.A. Water Air Soil Pollut. 152: 313-331.

Bindler R., Renberg I., Klaminder J., 2008. Bridging the gap between ancient metal pollution and contemporary biogeochemistry. J. Paleolimnol. 40: 755-770.

523 Biswas A., Blum J.D., Keeler G.J., 2008. Mercury storage in surface soils in a central
524 Washington forest and estimated release during the 2001 Rex Creek Fire. Sci. Total
525 Environ. 404: 129-138.

526 Blackwell B.D., Driscoll C.T., Maxwell J.A., Holsen T.M., 2014. Changing climate alters
527 inputs and pathways of mercury deposition to forested ecosystems. Biogeochemistry 119:
528 215-228.

529 Buurman P., Jongmans A.G., 2005. Podzolisation and soil organic matter dynamics.
530 Geoderma 125: 71-83.

531 Clarkson T.W., Magos L., 2006. The toxicology of mercury and its chemical compounds.
532 Crit. Rev. Toxicol. 36: 609-662.

533 De Coninck F., 1980. Major mechanisms in formation of spodic horizons. Geoderma 24:
534 101-128.

535 Do Valle C.M., Santana G.P., Augusti R., Egreja-Filho F.B., Windmöller C.C., 2005.
536 Speciation and quantification of mercury in oxisol, ultisol, and spodosol from Amazon
537 (Manaus, Brazil). Chemosphere 58: 779-792.

538 Driscoll C.T., Mason R.P., Chan H.M., Jacob D.J., Pirrone N., 2013. Mercury as a global
539 pollutant: Sources, pathways, and effects. Environ. Sci. Technol. 47: 4967-4983.

540 Ferro-Vázquez C., Nóvoa-Muñoz J.C., Costa-Casais M., Klaminder J., Martínez-Cortizas
541 A., 2014. Metal and organic matter immobilization in temperate podzols: a high
542 resolution study. Geoderma 217-218: 225-234.

543 Ferro-Vázquez C., Pérez-Rodríguez M., Nóvoa-Muñoz J.C., Klaminder J., Bindler R.,
544 Martínez Cortizas A., 2017. Tracing Pb pollution penetration in temperate podzols. Land
545 Degrad. Dev. 28: 2432-2445.

546 Frossard A., Hartmann M., Frey B., 2017. Tolerance of the forest soil microbiome to
547 increasing mercury concentrations. Soil Biol. Biochem. 105: 162-176.

548 Gabriel M.C., Williamson D.G., 2004. Principal biogeochemical factors affecting the
549 speciation and transport of mercury through the terrestrial environment. Environ.
550 Geochem. Health 26: 421-434.

551 Gómez-Armesto A.G., Bibián-Núñez L., Campillo-Cora C., Pontevedra-Pombal X.,
552 Arias-Estévez M., Nóvoa-Muñoz J.C., 2018. Total mercury distribution among soil
553 aggregate size fractions in a temperate forest podzol. Span. J. Soil. Sci. 8: 57-73.

554 Grigal D.F., 2003. Mercury sequestration in forests and peatlands: A review. J. Environ.
555 Qual. 32: 393-405.

556 Grimaldi C., Grimaldi M., Guedron S., 2008. Mercury distribution in tropical soil profiles
557 related to origin of mercury and soil processes. Sci. Total Environ. 401: 121-129.

558 Guedron S., Grangeon S., Lanson B., Grimaldi M., 2009. Mercury speciation in a tropical
559 soil association; consequence of gold mining on Hg distribution in French Guiana.
560 Geoderma 153: 331-346.

561 Guedron S., Grimaldi C., Chauvel C., Spadini L., Grimaldi M., 2006. Weathering versus
562 atmospheric contributions to mercury concentrations in French Guiana soils. Appl.
563 Geochem. 21: 2010-2022.

564 Gustin M.S., Lindberg S.E., Weisberg P.J., 2008. An update on the natural sources and
565 sinks of atmospheric mercury. Appl. Geochem. 23: 482-493.

566 Hissler C., Probst J., 2006. Impact of mercury atmospheric deposition on soils and
567 streams in a mountainous catchment (Vosges, France) polluted by chlor-alkali industrial

568 activity: The important trapping role of the organic matter. Sci. Total Environ. 361: 163-
569 178.

570 Jiskra M., Wiederhold J.G., Skyllberg U., Kronberg R., Hajdas I., Kretzschmar R., 2015.
571 Mercury deposition and re-emission pathways in boreal forest soils investigated with Hg
572 isotope signatures. Environ. Sci. Technol. 49: 7188-7196.

573 Juillerat J.I., Ross D.S., Bank M.S., 2012. Mercury in litterfall and upper soil horizons in
574 forested ecosystems in Vermont, USA. Environ. Toxicol. Chem. 31: 1720-1729.

575 Khwaja A.R., Bloom P.R., Brezonik P.L., 2006. Binding constants of divalent mercury
576 (Hg^{2+}) in soil humic acids and soil organic matter. Environ. Sci. Technol. 40: 844-849.

577 Larssen T., de Wit H.A., Wiker M., Halse K., 2008. Mercury budget of a small forested
578 boreal catchment in southeast Norway. Sci. Total Environ. 404: 290-296.

579 Manceau A., Nagy K.L., 2008. Relationships between Hg(ii)-S bond distance and Hg(ii)
580 coordination in thiolates. Dalton Trans. 11: 1421-5.

581 Martínez-Cortizas A., Peiteado-Varela E., Bindler R., Biester H., Cheburkin A., 2012.
582 Reconstructing historical Pb and Hg pollution in NW Spain using multiple cores from the
583 Chao de Lamoso bog (Xistral Mountains). Geoch. Cosmoch. Acta 82: 68-78.

584 Mitchell C.P.J., Branfireun B.A., Kolka R.K., 2008. Total mercury and methylmercury
585 dynamics in upland-peatland watersheds during snowmelt. Biogeochemistry 90: 225-
586 241.

587 Navrátil T., Shanley J., Rohovec J., Hojdová M., Penížek V., Buchtová J., 2014.
588 Distribution and pools of mercury in Czech forest soils. Water Air Soil Pollut. 225: 1829.

589 Obrist D., Johnson D.W., Lindberg S.E., Luo Y., Hararuk O., Bracho R., Battles J.J., Dail
590 D.B., Edmonds R.L., Monson R.K., Ollinger S.V., Pallardy S.G., Pregitzer K.S., Todd

591 D.E., 2011. Mercury distribution across 14 U.S. Forests. Part I: Spatial patterns of
592 concentrations in biomass, litter, and soils. Environ Sci. Technol. 45: 3974-3981.

593 Obrist D., 2012. Mercury distribution across 14 U.S. forests. Part II: Patterns of methyl
594 mercury concentrations and areal mass of total and methyl mercury. Environ Sci.
595 Technol. 46: 5921-5930.

596 Obrist D., Pearson C., Webster J., Kane T., Lin C., Aiken G.R., Alpers C.N., 2016. A
597 synthesis of terrestrial mercury in the western United States: Spatial distribution defined
598 by land cover and plant productivity. Sci. Total Environ. 568: 522-535.

599 Peña-Rodríguez S., Pontevedra-Pombal X., Gayoso E.G.R., Moretto A., Mansilla R,
600 Cutillas-Barreiro L., Arias-Estévez M., Nóvoa-Muñoz J.C., 2014. Mercury distribution
601 in a toposequence of sub-Antarctic forest soils of Tierra del Fuego (Argentina) as
602 consequence of the prevailing soil processes. Geoderma 232-234: 130-140.

603 Regnell O., Watras C.J., 2019. Microbial Mercury Methylation in Aquatic Environments:
604 A Critical Review of Published Field and Laboratory Studies. Environ Sci. Technol. 53:
605 4-19.

606 Richardson J.B., Aguirre A.A., Buss H.L., Toby O'Geen A., Gu X., Rempe D.M., Rempe
607 D.M., Richter D.B, 2018. Mercury Sourcing and Sequestration in Weathering Profiles at
608 Six Critical Zone Observatories. Global Biogeochem. Cycles 32: 1542-1555.

609 Richardson J.B., Friedland A.J., Engerbretson T.R., Kaste J.M., Jackson B.P., 2013.
610 Spatial and vertical distribution of mercury in upland forest soils across the northeastern
611 United States. Environ. Pollut. 182: 127-134.

612 Risch M.R., Dewild J.F., Krabbenhoft D.P., Kolka R.K., Zhang L., 2012. Litterfall
613 mercury dry deposition in the eastern USA. Environ. Pollut. 161: 284-290.

614 Rózanski S.L., Castejón J.M.P., Fernández G.G., 2016. Bioavailability and mobility of
615 mercury in selected soil profiles. Environ. Earth Sci. 75:1065.

616 Sauer D., Sponagel H., Sommer M., Giani L., Jahn R., Stahr K., 2007. Podzol: Soil of the
617 year 2007. A review on its genesis, occurrence, and functions. J. Plant Nutr. Soil Sci. 170:
618 581-597.

619 Schlüter K., 1997. Sorption of inorganic mercury and monomethyl mercury in an iron-
620 humus podzol soil of southern Norway studied by batch experiments. Environ. Geol. 30:
621 266-279.

622 Schlüter K., Gäth S., 1997. Modelling leaching of inorganic Hg(II) in a scandinavian iron-
623 humus podzol - Validation and long-term leaching under various deposition rates. Water
624 Air Soil Pollut. 96: 301-320.

625 Schroeder W.H., Munthe J., 1998. Atmospheric mercury - An overview. Atmos. Environ.
626 32: 809-822.

627 Schwesig D., Matzner E., 2000. Pools and fluxes of mercury and methylmercury in two
628 forested catchments in Germany. Sci, Total Environ. 260: 213-223.

629 Schwesig D., Kalbitz K., Matzner E., 2003. Effects of aluminium on the mineralization
630 of dissolved organic carbon derived from forest floors. Eur. J. Soil Sci. 54: 311-322.

631 Skyllberg U., Bloom P.R., Qian J., Lin C., Bleam WF., 2006. Complexation of
632 mercury(II) in soil organic matter: EXAFS evidence for linear two-coordination with
633 reduced sulfur groups. Environ Sci. Technol. 40: 4174-4180.

634 Smith-Downey N.V., Sunderland E.M., Jacob D.J., 2010. Anthropogenic impacts on
635 global storage and emissions of mercury from terrestrial soils: Insights from a new global
636 model. J. Geophys. Res. Biogeosci. 115.

637 Sunderland E.M., Mason R.P., 2007. Human impacts on open ocean mercury
638 concentrations. Global Biogeochem. Cycles 21.

639 Nave L.E., Covarrubias Ornelas A., Drevnick P.E., Gallo A., Hatten J.A., Heckman K.A.,
640 Matosziuk L., Sanclements M., Strahm B.D., Veverica T.J., Weiglein T.L., Swanston
641 C.W., 2019. Carbon–mercury interactions in Spodosols assessed through density
642 fractionation, radiocarbon analysis, and soil survey information. Soil Sci. So.c Am. J. 83:
643 190-202.

644 Schwertmann U., Cornell R.M. Iron oxides in the laboratory: preparation and
645 characterization. VHC-Weinheim, New York 1991.

646 Tipping E., Lofts S., Hooper H., Frey B., Spurgeon D., Svendsen C., 2010. Critical Limits
647 for Hg(II) in soils, derived from chronic toxicity data. Environ. Pollut. 158: 2465-2471.

648 Xin M., Gustin M.S., 2007. Gaseous elemental mercury exchange with low mercury
649 containing soils: Investigation of controlling factors. Appl. Geochem. 22: 1451-1466.

650 Yu X., Driscoll C.T., Warby R.A.F., Montesdeoca M., Johnson C.E., 2014. Soil mercury
651 and its response to atmospheric mercury deposition across the northeastern United States.
652 Ecol. Appl. 24: 812-822.

653

654

655

656

657

658

659

660

661

Table 1. Mean values (± standard deviation) of some chemical properties of ACB-I and ACB-II soils on the basis of horizons identified in the field.

Soil	Hor	Depth	[a]n	[b]pH_K	[b]OM	[b]N	[c]SB	[c]Al_K	[d]Hg_T	[d]$\sum Hg_{TRes}$
					--------- g kg^{-1} ---------		------ $cmol_c$ kg^{-1} ------		µg kg^{-1}	mg m^{-2}
ACB-I	A	0-25	5	3.3 ± 0.2	68.7 ± 26.6	2.2 ± 0.7	0.6 ± 0.3	2.1 ± 0.6	28.0 ± 13.9	6.1
	E	25-55	6	3.5 ± 0.1	11.2 ± 4.1	0.5 ± 0.3	0.3 ± 0.0	0.7 ± 0.2	6.7 ± 2.2	2.6
	Bhs1	55-70	3	3.6 ± 0.3	50.0 ± 1.0	1.2 ± 0.1	0.7 ± 0.3	5.1 ± 2.1	34.3 ± 19.6	4.7
	Bhs2	70-95	5	4.4 ± 0.1	31.7 ± 4.5	0.9 ± 0.2	0.4 ± 0.1	1.9 ± 0.6	55.3 ± 12.5	15.1
	Bw	95-125	6	4.6 ± 0.0	14.7 ± 4.7	0.6 ± 0.3	0.4 ± 0.1	0.9 ± 0.2	29.6 ± 5.7	11.0
	BwC	125-140	3	4.7 ± 0.0	6.1 ± 0.9	0.3 ± 0.0	0.3 ± 0.1	0.6 ± 0.0	17.0 ± 1.5	3.4
ACB-II	A	0-15	3	3.2 ± 0.1	61.0 ± 3.8	1.5 ± 0.3	0.6 ± 0.2	1.2 ± 0.1	23.6 ± 6.3	2.7
	E	15-30	3	3.7 ± 0.1	8.7 ± 2.7	0.3 ± 0.1	0.2 ± 0.0	0.3 ± 0.1	5.6 ± 0.7	1.2
	Bhs1	30-40	2	3.8 ± 0.1	66.5 ± 39.6	2.0 ± 1.2	0.7 ± 0.3	4.8 ± 1.9	41.3 ± 34.4	3.8
	Bhs2	40-60	4	4.2 ± 0.2	33.8 ± 18.1	1.0 ± 0.5	0.5 ± 0.2	2.1 ± 0.9	63.0 ± 9.5	13.8
	Bw	60-90	6	4.3 ± 0.2	9.2 ± 3.6	0.5 ± 0.1	0.3 ± 0.1	1.2 ± 0.2	46.3 ± 7.3	18.9
	BwC	90-100	2	4.5 ± 0.0	6.1 ± 0.3	0.4 ± 0.1	0.4 ± 0.0	1.9 ± 0.0	39.8 ± 1.2	5.8

[a] n is the number of samples for each soil horizon

[b] pH_K is soil pH in saline solution (1 M KCl), OM is the total content of organic matter and N is the total nitrogen content

[c] SB is the sum of exchangeable base cations (Na, K, Ca and Mg) and Al_K is the exchangeable aluminium

[d] Hg_T and Hg_{TRes} are total mercury content and the mass of total Hg in areal basis for each whole horizon

Table 2. Loadings of the soil properties used in the PCA.

	PC1	PC2	PC3	PC4	Com
Fe_o	**0.88**	0.33	-0.11	0.11	0.91
Al_{La}	**0.86**	0.22	0.04	0.34	0.91
Fe_p	**0.86**	0.42	-0.06	0.07	0.93
Fe_T	**0.84**	0.31	0.29	0.00	0.88
Al_{ol}	**0.82**	0.41	-0.05	0.13	0.86
Fe_d	**0.79**	0.47	0.22	-0.07	0.89
Al_K	**0.76**	-0.08	0.11	0.50	0.85
C_p	**0.61**	0.35	-0.33	0.58	0.95
Al_o	0.35	**0.88**	0.24	0.03	0.96
Al_p	0.47	**0.84**	0.23	0.03	0.98
Al_{om}	0.43	**0.83**	0.12	0.21	0.94
Al_{oh}	0.42	**0.82**	0.25	-0.10	0.93
Al_{Cu}	0.56	**0.74**	0.12	0.27	0.95
Al_T	0.16	**0.69**	0.55	-0.28	0.88
pH_K	0.08	**0.67**	0.44	-0.49	0.89
Si_n	-0.04	0.27	**0.94**	-0.05	0.97
Al_c	0.14	0.10	**0.94**	-0.18	0.95
Si_c	-0.02	0.28	**0.94**	-0.02	0.97
Al_n	0.28	0.52	**0.78**	-0.11	0.97
Zr_T	-0.29	-0.44	**0.68**	-0.34	0.86
Fe_c	0.45	0.48	**0.49**	-0.24	0.74
N	0.09	-0.07	-0.11	**0.92**	0.88
C	0.22	-0.02	-0.27	**0.91**	0.94
Si_T	-0.53	-0.54	0.04	**-0.58**	0.90
Eigv	7.0	6.4	5.0	3.4	
Var	29.1	26.8	21.0	14.2	

PC1 – PC4: components
Com: communality, proportion of the variance of each parameter explained by the extracted components
Eigv: eigenvalue
Var: percentage of variance explained by each component

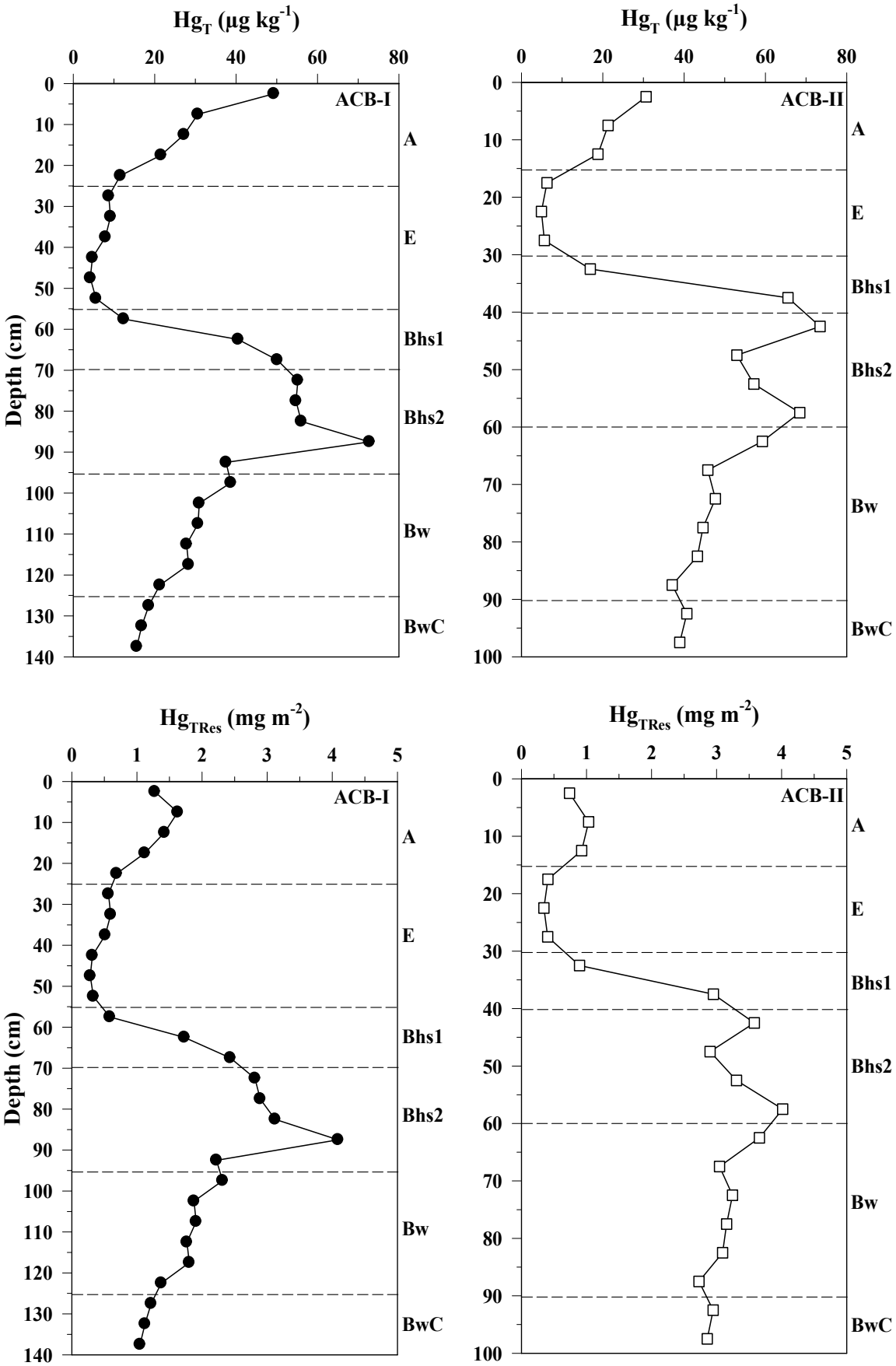

Figure 1. Total Hg (Hg_T) and total Hg pools (Hg_{TRes}) distribution in ACB-I and ACB-II.

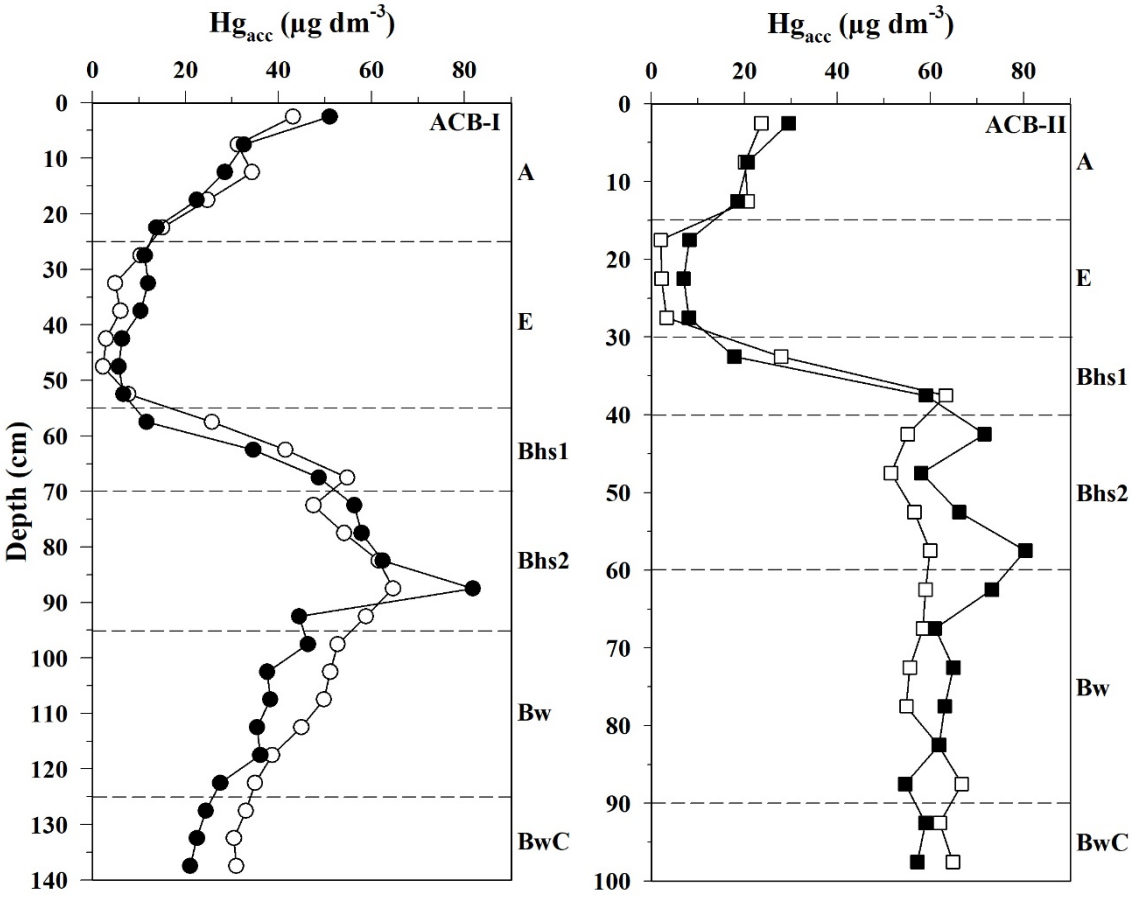

Figure 2. Distribution of observed (filed symbols) vs predicted Hg_{acc} (empty symbols) in ACB-I and ACB-II.

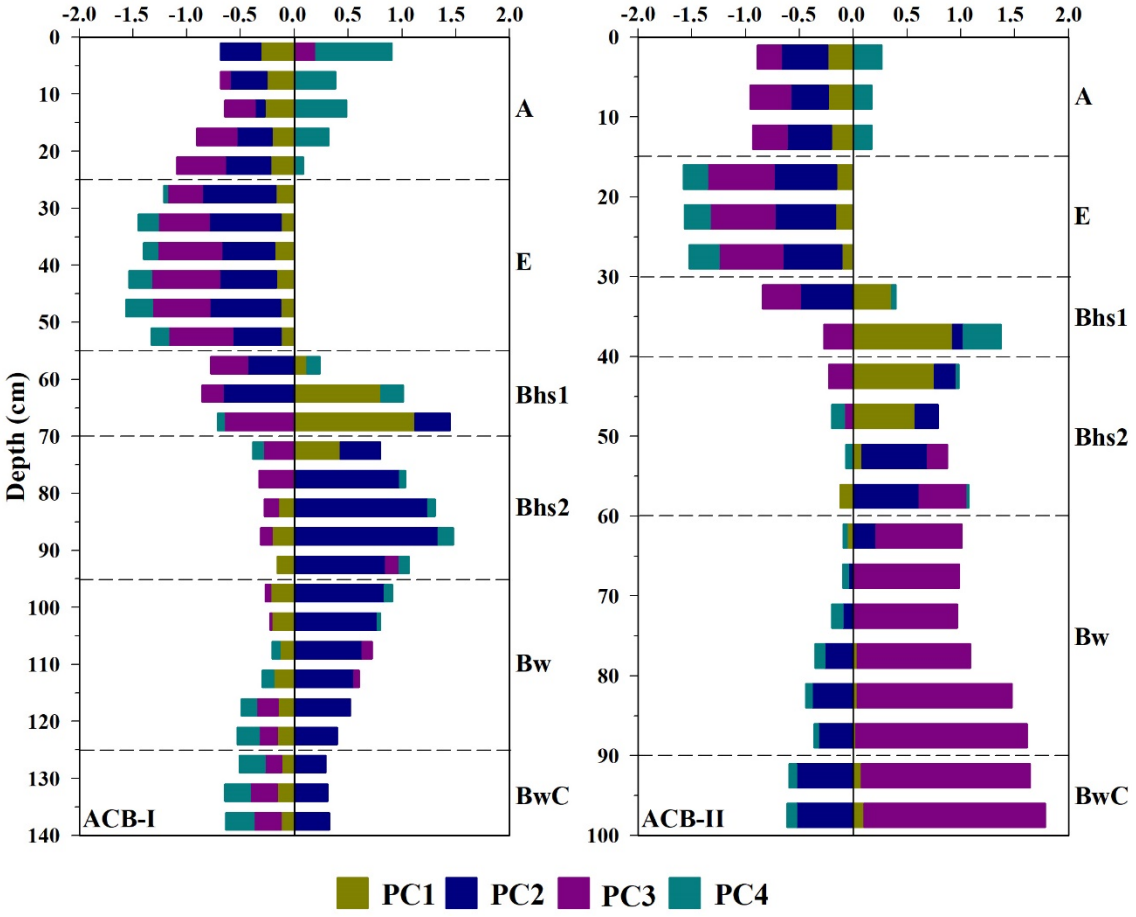

Figure 3. Contribution of each PC (wPC) to the predicted Hg_{acc} of each sample (weight: regression coefficient for a given component multiplied by the score of the component in each sample).

Declaration of interests

 The authors declare that they have no known competing financial interests or personal relationships that could have appeared to influence the work reported in this paper.

☐The authors declare the following financial interests/personal relationships which may be considered as potential competing interests:

Supplementary material for "Modelling Hg mobility in podzols: role of soil components and environmental implications"

Gómez-Armesto, Antía[ab*]; Martínez-Cortizas, Antonio[c]; Ferro-Vázquez, Cruz[d]; Méndez-López, Melissa[ab]; Arias-Estévez, Manuel[a]; Nóvoa-Muñoz, Juan Carlos[ab]

[a] Área de Edafoloxía e Química Agrícola, Departamento de Bioloxía Vexetal e Ciencia do Solo, Facultade de Ciencias, Universidade de Vigo. 32004 Ourense, España.

[b] Environmental Technology and Assessment Laboratory. Campus da Auga- Campus of Ourense. University of Vigo. 32004, Ourense, Spain.

[c] Eco-Past (GI-1553), Faculty of Biology, Universidade de Santiago de Compostela. 15782 Santiago, Spain.

[d] ICArEHB-Interdisciplinary Center for Archaeology of Human Behaviour. Faculty of Human and Social Sciences. University of Algarve. 8005-139 Faro, Portugal.

*Corresponding author: angomez@uvigo.es

Soil Hg pool estimation

The total Hg soil pool (Hg_{TRes}), which is an estimate of the absolute amount of Hg stored in a whole soil pedon, was estimated for each sample having into account the depth, soil bulk density and Hg concentration (Hg_T) according to Equation 1:

$$Hg_{TRes} = BD * P * Hg_T \qquad Eq.\ (1)$$

where BD is soil bulk density in Mg m^{-3} (Table S1), P is the depth in m and Hg_T is the total Hg content in mg Mg^{-1}. The soil Hg pool for each sample is expressed in mg m^{-2}.

General characteristics of the two profiles

Both soils have a sandy texture in A and E horizons (> 70 % sand) and loamy sand or sandy clay loam in the illuvial ones (Gómez-Armesto et al., 2018). Main chemical characteristics of the soils ACB-I and ACB-II are reported in detail in Ferro-Vázquez et al. (2014). In brief, the two soils are strong to moderately acid (water pH between 4.0 and 5.0) and total organic carbon (C) and total nitrogen (N) contents diminish with depth in both profiles (Table S1). The highest mean C content was found in the A horizon of ACB-I (40 g kg^{-1}) and in the Bhs1 horizon (39 g kg^{-1}) of ACB-II. Easily mineralized C, equivalent to C extracted with Na-pyrophosphate (C_p), peaks in Bhs1 horizons of both soils (24 g kg^{-1} for ACB-I and 21 g kg^{-1} for ACB-II). The effective cation exchange capacity (eCEC) is very low in both soils, varying between 0.6 and 5.8 $cmol_c$ kg^{-1}, and highly saturated in Al (Table S1). Aluminium fractionation is dominated by Al-humus complexes, whereas Fe fractionation is evenly distributed among crystalline and non-crystalline compounds, being the latest dominated by organically bound Fe. Maximum values of Al-humus complexes were found in Bhs2 horizon while Fe compounds peak in

Bhs1 horizon of both profiles, a distinctive characteristic of these soils as was reported by Ferro-Vázquez et al. (2014)

Table S1. Main chemical properties of ACB-I.

Sample	Depth	Hor	[a]BD	[b]pH_w	[b]pH_K	[c]C	[c]C_p	[c]N	[d]SB	[d]eCEC	[e]Al_K	[e]Al_{La}	[e]Al_{Cu}	[f]Al_{ol}	[f]Al_{om}	[f]Al_{oh}	[g]Al_p	[g]Al_o	[g]Al_n	[g]Al_{ia}	[g]Al_c	[g]Fe_p	[g]Fe_o	[g]Fe_d	[g]Fe_{ia}	[g]Fe_c	[g]Si_o	[g]Si_n	[h]Fe_T	[h]Al_T	[h]Si_T	[h]Zr_T	[i]Hg_T	[i]Hg_{TRes}	[i]Hg_{acc}
	cm		g cm^{-3}			------g kg^{-1}-------			----------cmol$_c$ kg^{-1}----------								----------g kg^{-1}----------										---------mg kg^{-1}---------				µg kg^{-1}	mg m^{-2}	µg dm^{-3}
ACB-I-1	0-5	A	1.03	3.9	3.0	60.0	16.7	3.1	0.8	3.3	2.5	3.1	8.9	0.7	5.7	2.0	1.0	1.2	1.1	0.2	0.0	0.8	0.7	1.8	0.0	1.0	0.1	0.6	4	26	299	206	49.3	1.3	51.0
ACB-I-2	5-10		1.06	4.1	3.2	36.9	13.3	2.0	0.7	2.8	2.1	2.0	8.2	0.0	6.2	3.8	1.1	1.1	1.0	0.0	0.0	1.0	0.8	1.8	0.0	1.0	0.1	0.4	4	30	338	250	30.6	1.6	32.5
ACB-I-3	10-15		1.05	3.9	3.4	46.6	13.7	2.5	1.0	3.3	2.3	3.2	12.3	0.9	9.0	5.4	1.6	1.6	1.5	0.0	0.0	0.8	0.7	1.4	0.0	0.7	0.1	0.2	4	34	324	172	27.2	1.4	28.5
ACB-I-4	15-20		1.04	4.0	3.3	38.0	10.6	2.0	0.5	2.9	2.4	2.8	9.9	0.3	7.1	1.8	1.0	1.2	1.1	0.2	0.0	0.4	0.4	1.1	0.0	0.7	0.1	0.1	3	32	355	226	21.6	1.1	22.4
ACB-I-5	20-25		1.19	4.3	3.4	17.8	6.1	1.2	0.3	1.4	1.1	1.4	3.9	0.3	2.5	1.6	0.5	0.6	0.6	0.2	0.0	0.2	0.2	0.7	0.0	0.5	0.1	0.2	2	29	413	185	11.6	0.7	13.8
ACB-I-6	25-30	E	1.29	4.2	3.4	10.0	4.4	1.1	0.3	1.0	0.7	0.9	2.1	0.1	1.3	1.7	0.4	0.4	0.4	0.0	0.0	0.2	0.1	0.5	0.0	0.4	0.1	0.1	2	25	452	309	8.7	0.6	11.3
ACB-I-7	30-35		1.30	4.3	3.5	7.6	4.1	0.3	0.3	1.0	0.7	0.7	1.6	0.0	0.9	2.2	0.3	0.4	0.4	0.0	0.0	0.2	0.1	0.5	0.0	0.4	0.1	0.1	2	24	457	286	9.2	0.6	12.0
ACB-I-8	35-40		1.30	4.1	3.5	7.4	3.7	0.5	0.3	1.0	0.7	0.5	2.1	0.0	1.6	1.2	0.3	0.4	0.3	0.1	0.0	0.1	0.1	0.4	0.0	0.3	0.1	0.1	3	25	412	207	7.9	0.5	10.3
ACB-I-9	40-45		1.35	4.7	3.6	4.8	3.1	0.3	0.3	0.8	0.6	0.4	1.2	0.0	0.8	1.6	0.2	0.3	0.3	0.0	0.0	0.1	0.1	0.3	0.0	0.2	0.1	0.1	2	26	460	193	4.7	0.3	6.3
ACB-I-10	45-50		1.35	4.2	3.6	3.3	2.5	0.3	0.2	0.8	0.5	0.6	0.9	0.0	0.3	1.6	0.2	0.3	0.3	0.1	0.0	0.1	0.1	0.4	0.0	0.4	0.1	0.1	2	25	487	248	4.2	0.3	5.7
ACB-I-11	50-55		1.18	4.3	3.6	6.0	3.7	0.5	0.3	1.5	1.2	1.5	2.9	0.3	1.5	1.6	0.4	0.5	0.5	0.0	0.0	0.2	0.2	1.0	0.0	0.8	0.1	0.1	3	48	428	202	5.6	0.3	6.6
ACB-I-12	55-60	Bhs1	0.94	4.3	3.4	20.3	13.2	1.1	0.4	4.7	4.2	6.8	11.8	2.6	5.0	4.6	1.5	1.6	1.7	0.1	0.1	1.6	1.2	1.6	0.0	0.4	0.1	0.2	8	81	316	218	12.4	0.6	11.7
ACB-I-13	60-65		0.85	4.1	3.5	33.8	28.9	1.2	1.0	8.4	7.4	12.1	25.0	4.7	12.9	10.6	3.3	2.9	4.1	0.0	1.1	8.4	8.6	9.5	0.2	0.9	0.1	0.4	71	73	169	142	40.5	1.7	34.6
ACB-I-14	65-70		0.97	4.4	4.0	32.9	28.7	1.2	0.7	4.3	3.6	8.6	25.8	5.0	17.2	41.2	6.1	6.1	7.2	0.0	1.1	26.4	21.6	28.3	0.0	6.7	0.1	0.3	68	72	159	151	50.1	2.4	48.7
ACB-I-15	70-75	Bhs2	1.02	4.6	4.3	20.5	16.5	0.8	0.6	3.3	2.7	5.5	23.9	2.8	18.4	32.5	5.2	5.2	6.4	0.0	1.2	12.2	8.5	25.0	0.0	16.5	0.1	0.4	24	76	265	151	55.2	2.8	56.3
ACB-I-16	75-80		1.06	4.6	4.4	19.4	15.5	0.8	0.5	2.7	2.2	4.6	24.9	2.4	20.3	34.0	5.2	5.0	6.9	0.0	1.9	7.8	4.0	11.2	0.0	7.1	0.1	0.4	21	94	226	142	54.7	2.9	57.9
ACB-I-17	80-85		1.11	4.6	4.5	18.0	14.3	0.7	0.4	2.0	1.6	3.5	24.9	1.9	21.4	37.3	5.7	5.5	7.7	0.0	2.1	6.1	3.5	10.5	0.0	7.0	0.1	0.6	17	91	227	162	56.0	3.1	62.4
ACB-I-18	85-90		1.12	4.7	4.5	20.1	16.4	0.8	0.4	2.0	1.6	3.7	24.8	2.2	21.0	41.7	5.9	6.0	8.0	0.1	2.0	6.0	3.4	7.4	0.0	4.1	0.1	0.6	18	96	214	173	72.8	4.1	81.8
ACB-I-19	90-95		1.18	4.8	4.5	14.0	11.1	1.2	0.3	1.4	1.2	3.6	15.8	2.4	12.2	33.3	4.3	4.8	7.0	0.5	2.2	4.9	2.6	6.8	0.0	4.2	0.1	0.6	16	85	253	189	37.5	2.2	44.4
ACB-I-20	95-100	Bw	1.20	4.8	4.5	12.7	10.4	1.1	0.2	1.3	1.1	2.9	16.7	1.8	13.8	29.0	4.1	4.3	6.0	0.2	1.7	4.3	2.6	5.6	0.0	3.1	0.1	0.6	14	71	304	172	38.7	2.3	46.3
ACB-I-21	100-105		1.21	4.6	4.6	10.5	8.4	1.0	0.4	1.4	1.0	2.7	14.2	1.6	11.5	28.6	3.9	4.0	5.5	0.1	1.5	4.5	2.5	6.0	0.0	3.5	0.1	0.6	14	73	309	164	31.0	1.9	37.5
ACB-I-22	105-110		1.25	4.6	4.6	8.9	6.4	0.5	0.5	1.4	0.9	2.8	14.1	1.9	11.3	22.5	3.3	3.6	5.2	0.2	1.7	3.9	2.5	6.4	0.0	4.0	0.1	0.6	14	85	275	216	30.7	1.9	38.2
ACB-I-23	110-115		1.27	4.6	4.7	7.3	6.1	0.4	0.3	1.1	0.8	1.8	12.9	1.0	11.1	20.4	3.0	2.9	4.3	0.0	1.4	3.1	2.0	6.4	0.0	4.5	0.1	0.6	13	72	320	214	27.8	1.8	35.4
ACB-I-24	115-120		1.27	4.4	4.7	6.7	5.5	0.4	0.3	1.1	0.8	1.8	11.7	1.0	9.9	19.0	2.8	2.8	4.1	0.1	1.2	3.0	2.0	6.8	0.0	4.8	0.1	0.4	12	64	298	184	28.3	1.8	36.1
ACB-I-25	120-125		1.29	4.4	4.7	5.2	4.1	0.3	0.4	1.1	0.7	1.4	9.7	0.7	8.3	17.7	2.5	2.5	3.7	0.0	1.2	2.5	1.6	6.8	0.0	5.2	0.1	0.4	11	64	346	193	21.3	1.4	27.5
ACB-I-26	125-130	BwC	1.31	4.5	4.7	4.2	3.2	0.3	0.5	1.1	0.6	1.6	8.6	0.9	7.0	17.1	2.3	2.1	3.2	0.0	1.0	2.3	1.5	6.6	0.0	5.1	0.1	0.4	11	69	349	215	18.6	1.2	24.3
ACB-I-27	130-135		1.34	4.6	4.7	3.3	3.0	0.3	0.2	0.8	0.6	1.1	7.4	0.6	6.2	15.1	2.0	2.0	3.0	0.0	1.0	2.0	1.4	6.4	0.0	5.0	0.1	0.4	10	63	335	168	16.8	1.1	22.5
ACB-I-28	135-140		1.34	4.6	4.7	3.2	2.8	0.3	0.2	0.8	0.6	1.3	6.9	0.7	5.6	14.5	1.9	2.0	3.0	0.0	1.1	2.1	1.4	8.0	0.0	6.6	0.1	0.4	10	68	339	138	15.6	1.0	21.0

[a] BD: bulk soil density
[b] pH_w and pH_K are pH values measured in distilled water and 0.1 M KCl, respectively
[c] C, C_p and N are total carbon content, Na-pyrophosphate extracted C and total nitrogen content, respectively
[d] SB and eCEC are base cations (Ca, Mg, Na, K) and effective Cation Exchange Capacity, respectively
[e] Al_K, Al_{La} and Al_{Cu} are Al extracted with potassium chloride (K), lanthanum chloride (La) and copper chloride (Cu), respectively
[f] Al_{ol}, Al_{om} and Al_{oh} are Al-humus complexes of low (ol), medium (om) and high-stability (oh), respectively
[g] Al_p (Fe_p), Al_o (Fe_o, Si_o), Al_n (Si_n) and Fe_d: Al (Fe) extracted with Na-pyrophosphate (p), Al (Fe, Si) ammonium oxalate-oxalic acid (o), Al (Si) extracted with Na hydroxide (n) and Fe extracted with Na-dithionite-citrate (d), respectively
Alia (Feia) and Alc (Fec) are inorganic non-crystalline Al (Fe) and secondary crystalline Al (Fe) compounds, respectively
[h] Fe_T, Al_T, Si_T and Zr_T are total Fe, Al, Si and Zr contents, respectively
[i] Hg_T, Hg_{TRes} and Hg_{acc} are total Hg concentration, total Hg pool and accumulated Hg, respectively

Table S1 (continuation). Main chemical properties of ACB-II.

Sample	Depth	Hor	[a]BD	[b]pH_w	[b]pH_K	[c]C	[c]C_p	[c]N	[d]SB	[d]eCEC	[e]Al_K	[e]Al_{La}	[e]Al_{Cu}	[f]Al_{ol}	[f]Al_{om}	[f]Al_{oh}	[g]Al_p	[g]Al_o	[g]Al_n	[g]Al_{ia}	[g]Al_c	[g]Fe_p	[g]Fe_o	[g]Fe_d	[g]Fe_{ia}	[g]Fe_c	[g]Si_o	[g]Si_n	[h]Fe_T	[h]Al_T	[h]Si_T	[h]Zr_T	[i]Hg_T	[i]Hg_{TRes}	[i]Hg_{acc}
	cm		g cm^{-3}			------g kg^{-1}-------			----------cmol$_c$ kg^{-1}----------								----------g kg^{-1}----------											---------mg kg^{-1}---------				µg kg^{-1}	mg m^{-2}	µg dm^{-3}
ACB-II-1	0-5	A	0.96	4.6	3.2	37.3	9.2	1.8	0.8	2.0	1.2	2.1	4.6	0.9	2.5	3.4	0.8	0.7	1.0	0.0	0.3	0.7	0.7	1.7	0.0	1.0	0.1	0.5	4	20	385	216	30.7	0.7	29.5
ACB-II-2	5-10		0.97	4.6	3.3	35.9	7.2	1.4	0.5	1.6	1.2	1.9	5.5	0.8	3.5	4.7	0.9	0.8	1.0	0.0	0.2	0.7	0.6	1.7	0.0	1.1	0.1	0.3	3	26	393	219	21.3	1.0	20.7
ACB-II-3	10-15		0.98	4.6	3.2	33.0	7.6	1.3	0.5	1.8	1.3	2.3	7.1	1.0	4.8	4.2	1.0	1.0	1.2	0.0	0.2	0.4	0.5	0.9	0.0	0.5	0.1	0.3	3	28	398	277	18.8	0.9	18.5
ACB-II-4	15-20	E	1.30	4.7	3.6	6.8	2.1	0.3	0.3	0.6	0.3	0.6	1.0	0.3	0.4	1.1	0.2	0.3	0.3	0.1	0.0	0.1	0.1	0.4	0.0	0.3	0.1	0.1	2	19	468	229	6.3	0.4	8.2
ACB-II-5	20-25		1.40	4.7	3.7	4.4	1.5	0.4	0.2	0.5	0.2	0.5	0.5	0.3	0.0	1.3	0.2	0.2	0.2	0.1	0.0	0.1	0.1	0.4	0.0	0.3	0.1	0.1	2	22	441	209	4.9	0.3	6.9
ACB-II-6	25-30		1.43	4.7	3.8	3.9	1.7	0.2	0.2	0.7	0.5	0.9	1.1	0.5	0.1	1.8	0.3	0.3	0.3	0.1	0.0	0.3	0.2	0.9	0.0	0.7	0.1	0.1	3	33	443	207	5.6	0.4	8.1
ACB-II-7	30-35	Bhs1	1.05	4.6	3.7	22.3	9.9	1.2	0.5	4.0	3.5	7.6	13.3	4.1	5.8	10.7	2.2	1.6	2.4	0.0	0.8	4.3	2.0	6.8	0.0	4.8	0.1	0.1	11	58	332	219	16.9	0.9	17.9
ACB-II-8	35-40		0.90	4.5	3.9	54.8	31.8	2.9	0.9	7.1	6.2	11.2	39.3	5.1	28.0	32.8	6.5	5.3	7.3	0.0	2.0	24.6	21.4	29.1	0.0	7.6	0.1	0.3	44	64	210	156	65.6	3.0	59.0
ACB-II-9	40-45	Bhs2	0.97	4.7	4.1	34.9	19.1	1.7	0.6	3.8	3.2	8.4	23.6	5.2	15.1	44.3	6.1	4.6	7.0	0.0	2.5	17.9	12.8	27.2	0.0	14.4	0.1	0.4	40	69	240	158	73.5	3.6	71.6
ACB-II-10	45-50		1.09	4.7	4.3	18.1	11.0	1.0	0.7	3.2	2.5	7.0	19.7	4.6	12.6	37.8	5.2	3.8	6.7	0.0	2.9	12.7	8.4	19.6	0.0	11.2	0.1	0.5	26	69	324	168	53.0	2.9	58.0
ACB-II-11	50-55		1.16	4.7	4.4	13.2	8.0	0.7	0.5	1.9	1.5	3.9	15.5	2.4	11.6	37.4	4.8	4.7	7.8	0.0	3.1	6.4	4.0	13.1	0.0	9.1	0.1	0.7	20	75	325	184	57.2	3.3	66.1
ACB-II-12	55-60		1.17	4.7	4.0	12.2	4.9	0.7	0.3	1.5	1.1	3.1	17.0	2.0	13.9	26.6	3.9	5.0	8.4	1.0	3.4	3.1	1.7	9.6	0.0	7.9	0.1	0.8	19	78	325	202	68.5	4.0	80.3
ACB-II-13	60-65	Bw	1.23	4.8	4.1	9.1	3.5	0.5	0.3	1.3	1.0	2.8	14.1	1.8	11.3	22.0	3.3	4.3	9.0	1.1	4.7	2.3	2.2	7.6	0.0	5.4	0.1	0.8	18	63	346	312	59.3	3.7	73.2
ACB-II-14	65-70		1.33	4.8	4.2	6.0	2.7	0.6	0.3	1.3	1.1	2.4	10.8	1.4	8.4	22.2	3.0	2.7	8.6	0.0	5.9	2.4	1.8	6.8	0.0	5.0	0.1	0.7	18	64	335	307	45.9	3.0	60.9
ACB-II-15	70-75		1.36	5.1	4.2	5.3	1.7	0.4	0.3	1.3	1.1	2.4	8.7	1.3	6.3	18.4	2.4	2.2	8.0	0.0	5.8	2.0	1.5	7.3	0.0	5.8	0.1	0.7	16	72	331	252	47.7	3.2	64.9
ACB-II-16	75-80		1.41	5.1	4.3	4.3	1.8	0.5	0.4	1.6	1.3	2.2	7.5	0.9	5.3	15.2	2.0	2.0	7.7	0.0	5.7	2.0	1.3	6.8	0.0	5.5	0.1	0.7	17	57	331	256	44.7	3.2	63.1
ACB-II-17	80-85		1.43	5.0	4.5	4.0	1.6	0.6	0.4	1.8	1.5	2.3	8.1	0.8	5.8	13.9	2.0	1.9	7.8	0.0	5.9	2.0	1.1	7.0	0.0	5.9	0.1	0.8	16	66	339	327	43.3	3.1	61.9
ACB-II-18	85-90		1.47	5.1	4.5	3.4	1.4	0.6	0.4	2.0	1.6	2.2	8.2	0.6	6.0	15.0	2.1	1.7	7.6	0.0	5.8	2.0	1.0	7.5	0.0	6.5	0.1	1.0	17	68	345	291	37.1	2.7	54.6
ACB-II-19	90-95	BwC	1.45	5.0	4.5	3.7	1.5	0.4	0.4	2.3	1.8	2.3	6.8	0.5	4.5	11.7	1.7	1.7	6.5	0.1	4.8	2.4	0.9	7.2	0.0	6.3	0.1	1.0	17	63	335	335	40.7	2.9	58.9
ACB-II-20	95-100		1.47	4.9	4.5	3.4	1.4	0.3	0.4	2.3	1.9	2.2	6.4	0.3	4.2	13.4	1.8	1.5	7.3	0.0	5.8	2.4	0.8	8.0	0.0	7.2	0.1	1.0	17	70	318	324	39.0	2.9	57.1

[a] BD: bulk soil density
[b] pH_w and pH_K are pH values measured in distilled water and 0.1 M KCl, respectively
[c] C, C_p and N are total carbon content, Na-pyrophosphate extracted C and total nitrogen content, respectively
[d] SB and eCEC are base cations (Ca, Mg, Na, K) and effective Cation Exchange Capacity, respectively
[e] Al_K, Al_{La} and Al_{Cu} are Al extracted with potassium chloride (K), lanthanum chloride (La) and copper chloride (Cu), respectively
[f] Al_{ol}, Al_{om} and Al_{oh} are Al-humus complexes of low (ol), medium (om) and high-stability (oh), respectively
[g] Al_p (Fe_p), Al_o (Fe_o, Si_o), Al_n (Si_n) and Fe_d: Al (Fe) extracted with Na-pyrophosphate (p), Al (Fe, Si) ammonium oxalate-oxalic acid (o), Al (Si) extracted with Na hydroxide (n) and Fe extracted with Na-dithionite-citrate (d), respectively
Alia (Feia) and Alc (Fec) are inorganic non-crystalline Al (Fe) and secondary crystalline Al (Fe) compounds, respectively
[h] Fe_T, Al_T, Si_T and Zr_T are total Fe, Al, Si and Zr contents, respectively
[i] Hg_T, Hg_{TRes} and Hg_{acc} are total Hg concentration, total Hg pool and accumulated Hg, respectively

Table S2. List of soil properties used in the principal component analyses carried out for ABC-I and ACB-II.

Parameter	Extraction procedure	Observations	Reference
pH_K	soil pH in 1 M KCl solution	measure of potential soil acidity	(Guitián & Carballas, 1976)
C	CHN analyser	total organic carbon content	
N	CHN analyser	total nitrogen content	
C_p	0.1 Na pyrophosphate	C in metal-humus complexes	(Bascomb, 1968)
Al_K	1 M KCl	exchangeable Al	(Lin and Coleman, 1960)
Al_{La}	0.33 M $LaCl_3$	Al weakly bound to soil organic matter in Al-humus complexes (include exchangeable Al)	(Hargrove and Thomas, 1981)
Al_{Cu}	0.5 M $CuCl_2$	Al moderate and weakly bound to soil organic matter in Al-humus complexes	(Juo and Kamprath, 1979)
Al_p	0.1 Na pyrophosphate	Al bound to soil organic matter	(Bascomb, 1968)
Al_o	0.2 M ammonium oxalate–oxalic acid (pH 3)	Al in non-crystalline compounds (including Al-humus complexes)	(Blakemore, 1978)
Al_n	0.5 M NaOH	total reactive Al in secondary crystalline and non-crystalline compounds (including Al-humus complexes)	(Borggaard, 1985)
Al_{ol}	Al_{La}-Al_K	low stability Al-humus complexes	(García-Rodeja et al., 2004)
Al_{om}	Al_{Cu}-Al_{La}	moderate stability Al-humus complexes	(García-Rodeja et al., 2004)
Al_{oh}	Al_p-Al_{Cu}	high stability Al-humus complexes	(García-Rodeja et al., 2004)
Al_c	Al_n-Al_o	Al in secondary crystalline compounds	(García-Rodeja et al., 2004)
Fe_p	0.1 Na pyrophosphate	Fe bound to soil organic matter	(Bascomb, 1968)
Fe_o	0.2 M ammonium oxalate–oxalic acid (pH 3)	Fe in non-crystalline compounds (including Fe-humus complexes)	(Blakemore, 1978)
Fe_d	Na-dithionite-citrate	free Fe in secondary crystalline and non-crystalline compounds (including Fe-humus complexes)	(Holmgren, 1967)
Fe_c	Fe_d-Fe_o	secondary crystalline Fe compounds (oxyhydroxides)	(García-Rodeja et al., 2007)
Si_n	0.5 M NaOH	total free Si pool (include Si in secondary crystalline and non-crystalline compounds)	(Borggaard, 1985)
Si_c	Si_n-Si_o	Si in opaline silica and 1:1 phyllosilicates	(García-Rodeja et al., 2007)
Al_T	EMMA-XRF	total Al content	(Cheburkin and Shotyk, 1996)
Fe_T	EMMA-XRF	total Fe content	(Cheburkin and Shotyk, 1996)
Si_T	EMMA-XRF	total Si content	(Cheburkin and Shotyk, 1996)
Zr_T	EMMA-XRF	total Zr content	(Cheburkin and Shotyk, 1996)

Table S3. Hg_{TRes} (mg m^{-2}) per horizon for ACB-I and ACB-II. The percentage of the contribution of each horizon to the total Hg stored in the soil is shown between brackets.

	ACB-I	**ACB-II**
A	6.1 (14)	2.7 (6)
E	2.6 (6)	1.2 (3)
Bhs1	4.7 (11)	3.8 (8)
Bhs2	15.1 (35)	13.8 (30)
Bw	11.0 (26)	18.9 (41)
BwC	3.4 (8)	5.8 (13)
Total	43.1	46.2

Table S4. Stepwise principal components regression models for predicted Hg_T.

Model	**Equation**	**Adjusted R^2**
1	38.0+14.4*PC3	0.384
2	38.0+14.4*PC3+12.7*PC2	0.695
3	38.0+14.4*PC3+12.7*PC2+7.5*PC1	0.803
4	38.0+14.4*PC3+12.7*PC2+7.5*PC1+4.8*PC4	0.845

References

Gómez-Armesto AG, Bibián-Núñez L, Campillo-Cora C, Pontevedra-Pombal X, Arias-Estévez M, Nóvoa-Muñoz JC. Total mercury distribution among soil aggregate size fractions in a temperate forest podzol. Span J Soil Sci 2018;8:57-73.

Ferro-Vázquez C, Nóvoa-Muñoz JC, Costa-Casais M, Klaminder J, Martínez-Cortizas A. Metal and organic matter immobilization in temperate podzols: A high resolution study. Geoderma 2014;217-218:225-34.